A novel multicopter with improved torque disturbance rejection through added angular momentum

Nathan Bucki · Mark W. Mueller

Received: date / Accepted: date

Abstract This paper presents a novel multicopter design with an additional momentum wheel. The added angular momentum reduces the vehicle's sensitivity to torque disturbances compared to a conventional multicopter. The mechanical design, coupled with intelligent feedback control, allows for operation of autonomous aerial systems in challenging environments where conventional designs may fail. Sensitivity to torque disturbances is shown to monotonically decrease with increasing angular momentum, and the effect scales such that a greater improvement in torque disturbance sensitivity is experienced by smaller vehicles. For a fixed vehicle size, a trade-off exists between the added torque disturbance rejection capability, the power required to carry the wheel's added mass, and the kinetic energy of the rotating wheel. A cascaded controller structure is proposed that accounts for the additional angular momentum and that accelerates or decelerates the momentum wheel to gain additional control authority in yaw. Theoretical results are validated experimentally using two vehicles of different scales. The proposed vehicle design is likely to be of value in situations where precision control is required in the face of large disturbances.

Keywords Aerial Systems · Disturbance Sensitivity · Resilience · Challenging environments · Design

1 Introduction

Multicopters are used to perform a variety of tasks such as aerial imaging, environmental monitoring, building inspection, and search and rescue. However, in challenging conditions multicopters may be unable to perform adequately, due to (e.g.) the danger posed by poor tracking performance. For example, multicopters may struggle in high wind shear environments, or environments with flying debris (e.g. hail storms).

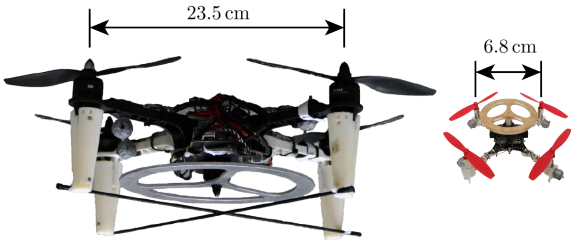

Fig. 1 Quadcopters of different sizes with added momentum wheels. Each momentum wheel is driven by a dedicated motor and spins about the thrust direction of the vehicle.

Several controllers have been developed that improve the disturbance rejection capabilities of multicopters. A method for estimating and compensating for wind disturbances acting on quadcopters was presented by Waslander and Wang (2009), and a sliding mode controller used in conjunction with a sliding mode disturbance observer was presented by Besnard et al. (2012) in order to improve robustness to unknown disturbances. Cabecinhas et al. (2014) use a nonlinear adaptive state feedback controller to track trajectories in the presence of constant force disturbances, and Zhang et al. (2011) develop an attitude controller and disturbance observer to compensate for time varying disturbances.

Although existing disturbance-observer-based controllers improve the disturbance rejection capabilities of the system, the performance of these controllers is inherently limited by the system dynamics, sensor noise,

N. Bucki
E-mail: nathan_bucki@berkeley.edu

M. W. Mueller
E-mail: mwm@berkeley.edu

and by the available range of control inputs. To improve disturbance rejection beyond what is possible by changing the controller, it is necessary to adapt the system's design. One such change is to increase the angular momentum in the thrust direction of the multicopter by attaching a momentum wheel that spins about the thrust axis of the multicopter (e.g. a momentum wheel as shown in Figure 1). The additional angular momentum aids in the rejection of torque disturbances, enhancing the ability of the vehicle to fly in environments with torque disturbances.

The idea of using angular momentum to improve attitude control was first rigorously studied in the context of dual-spin spacecraft, which are vehicles that consist of two bodies rotating about a shared spin axis in order to maintain a desired attitude. Attitude stability criteria for dual-spin spacecraft is presented in Likins (1967), and the effects of energy dissipation on dual-spin spacecraft is presented in Mingori (1969). However, the above consider the stabilizing effect of angular momentum on the orientation of spacecraft and do not focus on the effect of angular momentum on the translational dynamics of the vehicle.

Unlike a satellite in free-fall, the translation and orientation of a multicopter are strongly coupled, and thus the effect of angular momentum on the translational dynamics of multicopters must be considered in order to perform stable flight. Several multicopter-based vehicles have been proposed that exhibit stable flight with a significant amount of angular momentum. In Piccoli and Yim (2014), stability criteria are developed for a class of vehicles with a single propeller and passive stabilizing mechanisms, and the contribution of the vehicle's angular momentum to its stability is discussed. A method for controlling a quadcopter despite the loss of one, two, or three of its propellers is presented in Mueller and D'Andrea (2016) that involves the vehicle gaining significant angular momentum in order to hover, and this idea has been further investigated in Zhang et al. (2016), which presents an aerial vehicle that rotates parallel to the direction of gravity using only a single propeller. Furthermore, in Driessens and Pounds (2015) a novel aerial vehicle design is presented that uses one large propeller and three smaller propellers to enable more energy efficient flight compared to similar sized quadcopters. Due to the relative size and rotation directions of the propellers, the vehicle has a nonzero net angular momentum.

In this work we focus on how a large source of angular momentum can be used to enhance the torque disturbance rejection capabilities of a multicopter rather than treating any angular momentum as an unfortunate secondary effect of the vehicle design. In addition to these considerations, we emphasize the fact that for our proposed vehicle the effect of the momentum wheel can be changed mid-flight by changing the speed at which the wheel spins. Mid-flight changes to the dynamics of multicopters have also been explored, for example, in Ryll et al. (2013) and Wallace (2016). In Ryll et al. (2013) a quadcopter with tilting propellers is presented that is able to change the thrust direction of the vehicle without changing its attitude, and in Wallace (2016) a quadcopter capable of changing the length and orientation of its arms is presented. Although these vehicles are not specifically designed to improve the disturbance rejection capabilities of a multicopter, they allow the vehicle to perform maneuvers that a standard multicopter cannot.

This work builds on prior work (Bucki and Mueller, 2018), and extends it by adding

- an analysis of the disturbance rejection capabilities of the vehicle that includes position and velocity,
- a comparison between the force and torque disturbance rejection capabilities of the system,
- an analysis of how disturbance rejection scales with vehicle size,
- an analysis of the robustness of the control law to errors in the estimate of the total angular momentum of the vehicle,
- a new control law that leverages the source of angular momentum to improve the yaw control authority of the vehicle,
- additional experiments with a small scale quadcopter that verify how the disturbance rejection capabilities scale with vehicle size

This paper is organized as follows: Section 2 presents the nonlinear and linearized dynamics of the augmented system, Sect. 3 presents a disturbance rejection analysis and a discussion of trade-offs in the design of the momentum wheel, Sect. 4 describes a controller for the augmented system, and Sect. 5 presents experimental results.

2 Dynamics

In this section we present the dynamics of a vehicle with an added momentum wheel. We assume typical multicopter inputs, that is that the vehicle is capable of producing a thrust force along a single vehicle-fixed direction and three independent components of torque.

2.1 Notation

Non-bold symbols such as m represent scalars, lowercase bold symbols such as $\boldsymbol{g}$ represent vectors in $\mathbb{R}^3$,

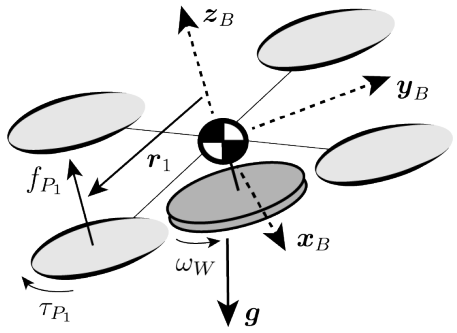

Fig. 2 Model of a quadcopter with an added momentum wheel. The momentum wheel rotates about $\boldsymbol{z}_B$ with angular velocity ω_W. Each propeller produces thrust force f_{P_i} and reaction torque τ_{P_i} about the propeller's axis of rotation at a displacement $\boldsymbol{r}_i$ from the center of mass of the vehicle.

and uppercase bold symbols such as $\boldsymbol{J}$ represent matrices in $\mathbb{R}^{3\times3}$. The short-hand notation (x, y, z) represents the elements of a vector. Subscripts such as m_W represent the body to which a quantity is related, and superscripts such as $\boldsymbol{g}^E$ represent an associated frame. The Earth-fixed frame is notated with E (and is assumed to be inertial), and the vehicle-fixed frame with B. The skew-symmetric matrix form of the cross product is written as $\boldsymbol{S}(\boldsymbol{a})$ such that $\boldsymbol{S}(\boldsymbol{a})\,\boldsymbol{b} = \boldsymbol{a} \times \boldsymbol{b}$. Angular velocities are written with two subscripts, with e.g. $\boldsymbol{\omega}^B_{BE}$ denoting the angular velocity of the body B with respect to the Earth E, expressed in the vehicle-fixed frame B. Identity matrices are written as I, with the dimension either clear from context or specified as a subscript.

2.2 System Dynamics

Figure 2 shows a model of a vehicle with an added momentum wheel. The momentum wheel is assumed to rotate about its center of mass, and the bodies are assumed rigid except for their relative rotation. The translational dynamics of the vehicle are derived using Newton's law (Zipfel, 2007), where the external forces are taken to be gravity $\boldsymbol{g}^E$ and the total propeller thrust force f_Σ, which acts along $\boldsymbol{z}^E_B$. Denoting the mass of the vehicle including the momentum wheel as m_Σ and the position of the vehicle center of mass with respect to a fixed point on the earth, expressed in the earth-fixed frame, as $\boldsymbol{d}^E_B$, the translational dynamics are then

$$m_\Sigma \ddot{\boldsymbol{d}}^E_B = m_\Sigma \boldsymbol{g}^E + \boldsymbol{z}^E_B f_\Sigma \tag{1}$$

The total mass moment of inertia of the vehicle (including the momentum wheel) is denoted $\boldsymbol{J}^B_\Sigma$, and the mass and mass moment of inertia of only the momentum wheel are denoted m_W and $\boldsymbol{J}^B_W$. We assume that the momentum wheel rotates about the vehicle-fixed thrust axis $\boldsymbol{z}_B$, and is symmetric about this axis of rotation, so that $\boldsymbol{J}^B_W$ is constant when expressed in the vehicle-fixed frame. The attitude dynamics may then be derived using Euler's law for clustered bodies with a fixed center of mass (Zipfel, 2007).

The vehicle rotates with respect to the earth at angular velocity $\boldsymbol{\omega}^B_{BE}$, written in the vehicle-fixed frame, and the wheel rotates with respect to the body at a speed ω_W so that $\boldsymbol{\omega}^B_{WB} = \boldsymbol{z}^B_B \omega_W$. The vehicle uses its propellers to produce an external torque $\boldsymbol{\tau}_u$, and an internal torque is produced by the motor driving the momentum wheel, which acts between the wheel and the body and is parallel to $\boldsymbol{z}_B$. Taking derivatives with respect to the vehicle-fixed frame, and manipulating, gives:

$$\begin{aligned}\boldsymbol{J}^B_\Sigma \dot{\boldsymbol{\omega}}^B_{BE} + \boldsymbol{J}^B_W \dot{\boldsymbol{\omega}}^B_{WB} = \\ - \boldsymbol{S}\big(\boldsymbol{\omega}^B_{BE}\big)\,\big(\boldsymbol{J}^B_\Sigma \boldsymbol{\omega}^B_{BE} + \boldsymbol{J}^B_W \boldsymbol{\omega}^B_{WB}\big) + \boldsymbol{\tau}^B_u\end{aligned} \tag{2}$$

Note that this neglects any effect due to the angular momentum of the propellers: Typical multicopters have an even number of propellers, identical up to a mirror symmetry, that rotate with alternating handedness, thus having near zero net angular momentum on average and having a negligible effect on the system dynamics. Moreover, the mass moment of inertia of the propellers is likely to be negligible compared to that of the body and momentum wheel. An example application where the propellers' angular momentum was considered significant is given in Mueller and D'Andrea (2014).

Compared to a traditional multicopter, the translational dynamics (1) are unchanged by the addition of the momentum wheel. However, the attitude dynamics include two additional terms: the coupling effect of the momentum wheel's angular momentum $\boldsymbol{S}\big(\boldsymbol{\omega}^B_{BE}\big)\,\boldsymbol{J}^B_W \boldsymbol{\omega}^B_{WB}$, and the acceleration/deceleration of the momentum wheel relative to the vehicle-fixed frame $\boldsymbol{J}^B_W \dot{\boldsymbol{\omega}}^B_{WB}$. Notably, the wheel coupling term is linear in the vehicle's angular velocity $\boldsymbol{\omega}^B_{BE}$, so that it has a much larger effect near hover than the other cross-coupling term $\boldsymbol{S}\big(\boldsymbol{\omega}^B_{BE}\big)\,\boldsymbol{J}^B_\Sigma \boldsymbol{\omega}^B_{BE}$ (which is quadratic with respect to $\boldsymbol{\omega}^B_{BE}$). The acceleration term $\dot{\boldsymbol{\omega}}^B_{WB}$ serves as additional control input to the system, and is actuated by the torque τ_W produced by the motor driving the momentum wheel. Note that because we neglect aerodynamic effects, the location of the momentum wheel in the $\boldsymbol{z}_B$ direction affects only the location of the center of mass and the total mass moment of inertia of the vehicle, and thus does not appear explicitly in the vehicle dynamics. The location of the center of mass relative to large aerodynamic surfaces may also affect a vehicle's stability, as is discussed in, e.g., Piccoli and Yim (2015).

The propeller torque and total force typically follow as a linear combination of the individual propeller forces f_{P_i}. For example, a quadcopter as shown in Fig. 2 has

$$f_\Sigma = \sum_{i=1}^{4} f_{P_i},\ \boldsymbol{\tau}_u^B = \sum_{i=1}^{4} \left(\boldsymbol{S}\left(\boldsymbol{r}_i^B\right) \boldsymbol{z}_B^B f_{P_i} + \boldsymbol{z}_B^B \kappa_i f_{P_i}\right) \quad (3)$$

where κ_i is a constant relating the aerodynamic drag to the thrust produced by the propellers, as is typical in multicopter models (e.g. Pounds et al. (2002)). For the remainder of this paper we will continue using the torque $\boldsymbol{\tau}_u$ and total force f_Σ as inputs, rather than the individual forces, as this will allow to decouple the system dynamics to first order, allowing for a cleaner presentation.

2.3 Linearized dynamics

Here we present the linearized system dynamics as background for the system analysis in the following section. When linearizing the system we assume that $\boldsymbol{x}_B$, $\boldsymbol{y}_B$, and $\boldsymbol{z}_B$ are the principal axes of inertia of both the vehicle and the momentum wheel. For simplicity of expression, we make the assumption that the vehicle has a 90° symmetry about its thrust axis, so that the moments of inertia about $\boldsymbol{x}_B$ and $\boldsymbol{y}_B$ are identical, and that the momentum wheel is symmetric about its axis of rotation. The principal mass moments of inertia about $\boldsymbol{x}_B$ and $\boldsymbol{z}_B$ are then denoted $J_{\Sigma,xx}$ and $J_{\Sigma,zz}$ respectively for the vehicle and $J_{W,xx}$, and $J_{W,zz}$ for the momentum wheel.

The position of the vehicle relative to a fixed point in the inertial frame is written as $\boldsymbol{d}_B^E = (x, y, z)$, and the velocity is written as $\dot{\boldsymbol{d}}_B^E = (\dot{x}, \dot{y}, \dot{z})$. The attitude of the vehicle relative to the inertial frame is written as roll, pitch, and yaw (notated ϕ, θ, ψ), and the angular velocity of the vehicle is written as $\boldsymbol{\omega}_{BE}^B = (p, q, r)$ where p, q and r are the body rates of the vehicle about the $\boldsymbol{x}_B$, $\boldsymbol{y}_B$, and $\boldsymbol{z}_B$ axes respectively. The dynamics are linearized about a desired angular velocity of the momentum wheel $\bar{\omega}_W$ such that $\Delta\omega_W = \omega_W - \bar{\omega}_W$ is the deviation of the angular velocity of the rotating body from the desired value.

The control inputs to the system are the deviation from the total thrust required to hover $\Delta f_\Sigma = f_\Sigma - m_\Sigma||\boldsymbol{g}||$, torques produced by the propellers $\boldsymbol{\tau}_u^B = (\tau_x, \tau_y, \tau_z)$, and the internal torque produced by the motor driving the momentum wheel τ_W. The linearization of (1) and (2) yields three decoupled subsystems with the following state and input vectors, where $\dot{s}_{xy} = A_{xy}s_{xy} + B_{xy}u_{xy}$, $\dot{s}_z = A_z s_z + B_z u_z$, and $\dot{s}_\psi = A_\psi s_\psi + B_\psi u_\psi$, and

$$s_{xy} = (x, y, \dot{x}, \dot{y}, \phi, \theta, p, q) \qquad u_{xy} = (\tau_x, \tau_y) \quad (4)$$

$$s_z = (z, \dot{z}) \qquad u_z = \Delta f_\Sigma \quad (5)$$

$$s_\psi = (\psi, r, \Delta\omega_W) \qquad u_\psi = (\tau_z, \tau_W) \quad (6)$$

The system matrices for these three linear subsystems are then

$$A_{xy} = \begin{bmatrix} 0 & I & 0 & 0 \\ 0 & 0 & A_1 & 0 \\ 0 & 0 & 0 & I \\ 0 & 0 & 0 & A_2 \end{bmatrix} \qquad B_{xy} = \begin{bmatrix} 0 \\ 0 \\ 0 \\ J_{\Sigma,xx}^{-1} I_{2\times 2} \end{bmatrix} \quad (7)$$

$$A_z = \begin{bmatrix} 0 & 1 \\ 0 & 0 \end{bmatrix} \qquad B_z = \begin{bmatrix} 0 \\ m_\Sigma^{-1} \end{bmatrix} \quad (8)$$

$$A_\psi = \begin{bmatrix} 0 & 1 & 0 \\ 0 & 0 & 0 \\ 0 & 0 & 0 \end{bmatrix} \qquad B_\psi = \begin{bmatrix} 0 & 0 \\ J_{\Sigma,zz}^{-1} & -J_{W,zz}^{-1} \\ 0 & J_{W,zz}^{-1} \end{bmatrix} \quad (9)$$

where

$$A_1 = ||\boldsymbol{g}|| \begin{bmatrix} 0 & 1 \\ -1 & 0 \end{bmatrix}, \quad A_2 = \frac{J_{W,zz}}{J_{\Sigma,xx}} \bar{\omega}_W \begin{bmatrix} 0 & -1 \\ 1 & 0 \end{bmatrix} \quad (10)$$

The linearized dynamics of the proposed system differ from the linearized dynamics of a normal multicopter due to the cross-coupling effect of matrix A_2, the additional state related to the wheel speed $\Delta\omega_W$, and the additional control input τ_W. When the nominal angular velocity of the momentum wheel $\bar{\omega}_W$ is zero, A_{xy} further decouples into a subsystem containing states $(x, \dot{x}, \theta, q)$ and a subsystem containing $(y, \dot{y}, \phi, p)$. However, as $\bar{\omega}_W$ increases in magnitude, the roll and pitch states becoming increasingly coupled, introducing an oscillatory mode into the dynamics that results in gyroscopic precession of the vehicle when external roll and pitch torques are applied. We show in the following section how this coupling improves the torque disturbance rejection capabilities of the vehicle as $\bar{\omega}_W$ increases when the additional angular momentum of the wheel is taken into account in the controller of the vehicle.

The additional control input τ_W is significant because it improves the yaw control authority of the vehicle. However its use causes deviation from the desired wheel speed, creating a trade-off between the improvement of the yaw control of the vehicle and the change in the magnitude of the coupling terms in A_2.

3 System analysis and design

In this section we first analyze how the sensitivity of the vehicle's horizontal motion to disturbances changes with respect to the scale of the vehicle and speed of the

wheel. We also examine the trade-off in the wheel design, comparing the power required to carry the wheel, the rotational energy that must be stored in the wheel, and the size of the wheel.

3.1 Scaling analysis

We compare the sensitivity of a system to external disturbances as the system size is varied, and reason about how all parameters scale as a function of the vehicle's size. Through this, we argue that smaller vehicles are likely to see a lower sensitivity to torque disturbances through the addition of a momentum wheel.

Noting that the system dynamics, to first order, decouple into horizontal, vertical, and yaw subsystems, we restrict our analysis to the horizontal subsystem where the momentum wheel affects the system dynamics. The scale of the vehicle is captured by a linear scaling factor λ, so that all lengths of the vehicle scale proportionally to λ.

3.1.1 Scaling of dynamics

Considering the linearized horizontal dynamics of (7), we note that the dynamics matrix A_{xy} is a function of the vehicle parameters only through the term $\frac{J_{W,zz}}{J_{\Sigma,xx}}\bar{\omega}_W$, while the input matrix B_{xy} contains only the inertia $J_{\Sigma,xx}^{-1}$.

Assuming materials of constant density are used, the mass of the vehicle will scale proportional to its volume, or $\sim \lambda^3$, and the mass moment of inertia of the vehicle as λ^5 (being composed of mass multiplied by distance squared). We assume that the added momentum wheel scales in the same manner as the rest of the vehicle's mass moment of inertia, so that the ratio $J_{W,zz}/J_{\Sigma,xx}$ is independent of λ.

The final parameter in the dynamics is the speed of the wheel, $\bar{\omega}_W$, which is here assumed to scale proportionally to the speed of the propellers. This assumption is motivated by the fact that the momentum wheel is likely to be powered by a motor similar to that powering the propellers, and that the energy stored in the momentum wheel during operation then scales proportionally to the energy stored in the propellers (so that the momentum wheel never represents a disproportionate amount of energy in the system). Inspired by Kushleyev et al. (2013) we apply Mach scaling to the propellers, assuming that the propeller tip speed remains constant at different scales, so that $\bar{\omega}_W \sim \lambda^{-1}$.

3.1.2 Scaling of controller parameters

We reason about the system's performance when rejecting disturbances by computing the system's closed-loop sensitivity to both torque and force disturbances when applying the $\mathcal{H}_2$ optimal controller (Green and Limebeer, 1995). The controller is parametrized through the costs applied to the error signal $z_{xy} \in \mathbb{R}^4$ defined as:

$$z_{xy} = c(\lambda)\begin{bmatrix} I_{2\times 2} & 0_{2\times 6} \\ 0_{2\times 2} & 0_{2\times 6} \end{bmatrix} s_{xy} + d(\lambda)\begin{bmatrix} 0_{2\times 2} \\ I_{2\times 2} \end{bmatrix} u_{xy} \tag{11}$$

where $c(\lambda)$ is the cost of position errors, and $d(\lambda)$ is the cost of applying inputs. Under the assumption that position errors are best measured in body-lengths, the cost factor will scale as $c(\lambda) \sim \lambda^{-1}$.

The cost applied to the input is assumed to scale inversely proportionally to the maximum torque that the vehicle can apply, which will scale as the maximum force multiplied by the linear scale. We assume that the maximum force scales as the vehicle's mass, so that the maximum torque scales as λ^4 and thus the cost as $d(\lambda) \sim \lambda^{-4}$.

3.1.3 Sensitivity to scaling

Under the preceding assumptions, the effect of adding a momentum wheel for disturbance rejection can be compared for vehicles of different sizes. We consider the effect of force as well as torque disturbances on the vehicle, but consider these effects separately: The relative magnitude of these disturbances will depend on the nature of the disturbances, the vehicle geometry, and other factors that are difficult to capture in a straight-forward scaling law. Torque disturbances enter as added to the torque inputs, and force disturbances act directly on the vehicle velocity state. As we will normalize performance at each scale, the dependence of these disturbances on vehicle scale is immaterial.

Specifically, we consider a vehicle of nominal parameters corresponding to the larger quadcopter shown in Fig. 1, where for $\lambda = 1$ we have $m_\Sigma = 922\,\mathrm{g}$, $J_{W,zz}/J_{\Sigma,xx} = 0.11$, $\bar{\omega}_W(\lambda) = 468\lambda^{-1}\mathrm{rad\,s^{-1}}$, and we use the costs $c(\lambda) = \lambda^{-1}\mathrm{m}^{-1}$, and $d(\lambda) = \lambda^{-4}\mathrm{N}^{-1}\,\mathrm{m}^{-1}$. Though these costs are chosen to illustrate the effect of scaling, the resulting feedback gain matrix is similar to that which is used in the experimental evaluation of Sect. 5, thus yielding meaningful insights.

The sensitivity to torque and force disturbances as a function of the momentum wheel speed at three different vehicle scales is shown in Fig. 3. The figure compares the nominal vehicle to vehicles that are of the scale $\lambda \in \left\{\frac{1}{2}, 1, 2\right\}$, i.e. with masses ranging from 115g to 7.4kg. The sensitivity to disturbances is defined as

the normalized state feedback $\mathcal{H}_2$ norm of the system, which can be interpreted as the signal energy of z_{xy} (defined in (11)) after Dirac impulse disturbances occur, written as

$$||z_{xy}||_2 = \left(\int_0^\infty z_{xy}(t)^T z_{xy}(t) dt \right)^{1/2} \tag{12}$$

Notable is that, for all scales, the vehicle's sensitivity to torque decreases monotonically with increasing momentum wheel speed. The sensitivity to force disturbances initially decreases weakly with increasing angular momentum, before increasing, so that vehicles with large added angular momentum may be more sensitive to force disturbances. Thus, a substantial decrease in sensitivity to torque disturbances may be achieved without a great change to sensitivity to force disturbances, and the exact trade-off will depend on the relative magnitudes of force disturbances and torque disturbances.

The smaller scale vehicle, moreover, is capable of storing more angular momentum in the wheel relative to the vehicle inertia, and thus has a lower overall sensitivity to torque disturbances at the expense of a higher sensitivity to force disturbances when compared to larger scale vehicles. Note, however, that such a comparison between vehicle scales relies on strong assumptions about how the dynamics and control parameters scale as described in the previous subsections.

An optimal choice for the trade-off between sensitivity to force and torque disturbances will require additional information about the nature of the expected disturbances, which are likely application-specific. Any practical design must also weigh the potential increase in system robustness to the additional cost of carrying the added mass of the momentum wheel. This is touched upon next.

3.2 Momentum wheel design

For a fixed sized vehicle, we now investigate the design of the momentum wheel itself. Specifically, a designer must choose a wheel size, mass, and angular velocity; these will be shown to relate to the vehicle's efficiency, safety, and disturbance sensitivity.

The benefit to the dynamics follows from the angular momentum of the wheel, $J_{W,zz}\omega_W$, so that the effect is increased with increasing momentum. Increasing the wheel mass increases its mass moment of inertia, but this requires additional power to be carried. The increase in power consumption at hover due to the added weight can be estimated through momentum theory, which holds that the total mechanical power produced

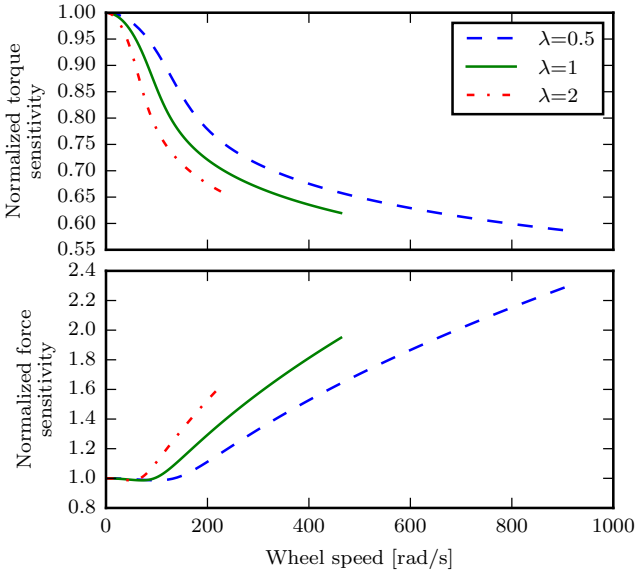

Fig. 3 Normalized ability to reject disturbances at three different vehicle scales λ. Sensitivities are computed under the assumptions of Sect. 3.1.3. As the scale of the vehicle decreases, the normalized torque disturbance sensitivity of the vehicle decreases and the normalized force sensitivity of the vehicle increases.

by the propellers P_Σ is related to the mass of the vehicle as $P_\Sigma = \mu m_\Sigma^{3/2}$, where μ is an experimentally measured constant that depends on the propeller geometry (McCormick, 1995). The maximum moment of inertia for a given mass is provided by a thin ring, whose outer radius will typically be constrained by mechanical considerations of the vehicle (e.g. so that the wheel does not protrude beyond the vehicle arms). For maximum efficiency, thus, a wheel of low mass but large radius is desired.

The momentum may also be increased by increasing the wheel's speed, but the added kinetic energy may represent a substantial safety concern e.g. in the event of a crash. For a fixed angular momentum and wheel size, the kinetic energy stored in the rotating wheel $\frac{1}{2} J_{W,zz} \omega_W^2$ increases inversely proportionally to the mass of the wheel. If, instead, the wheel mass and angular momentum are fixed, but its radius and speed are allowed to vary, the energy stored scales inversely proportionally to the radius squared. A practical design must trade off the additional power required to lift the wheel, the energy stored in the wheel, the radius of the wheel, and the vehicle's disturbance sensitivity.

4 Control

We next propose a specific cascaded control strategy for the vehicle, separating position and attitude control. Unlike the system at hover, the proposed cascaded

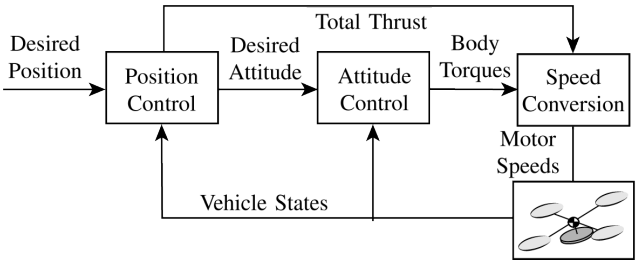

Fig. 4 Proposed cascaded controller architecture.

controller is straightforwardly able to cope with large changes of the vehicle's attitude. Although the proposed cascaded controller has a slightly larger $\mathcal{H}_2$ cost than a naïve application of the full-state linearized controller, it is shown to have much improved robustness to error in the estimated momentum wheel speed.

For the controller, an outer (position) controller computes a desired total thrust f_Σ and thrust direction to track position reference commands, and an inner (attitude) controller tracks this desired thrust direction and a yaw command by commanding desired torques $\boldsymbol{\tau}_u^B$ and a desired internal torque on the wheel τ_W. The total force and torques are finally converted to individual motor speed commands. This is shown in Fig. 4.

We proceed by defining state feedback $\mathcal{H}_2$ optimal position and attitude controllers based on the linearized dynamics derived in Sect. 2.3. An analytic expression for the state feedback $\mathcal{H}_2$ optimal attitude controller based on the estimated speed of the momentum wheel is given, allowing for the $\mathcal{H}_2$ optimal attitude controller to be computed on-the-fly at low computational cost during quasi-static wheel speed changes.

4.1 Position control

Let $\boldsymbol{d}_{B,e}^E$ represent the difference between the desired and current position, $\dot{\boldsymbol{d}}_{B,e}^E$ represent the difference between the desired and current velocity, and $\ddot{\boldsymbol{d}}_{B,d}^E$ represent the desired acceleration of the vehicle. The linear system $\dot{s}_p = A_p s_p + B_p u_p$ is then defined as follows

$$s_p = (\boldsymbol{d}_{B,e}^E, \dot{\boldsymbol{d}}_{B,e}^E), \qquad u_p = \ddot{\boldsymbol{d}}_{B,d}^E \tag{13}$$

$$A_p = \begin{bmatrix} 0 & I \\ 0 & 0 \end{bmatrix}, \qquad B_p = \begin{bmatrix} 0 \\ I \end{bmatrix} \tag{14}$$

This linear system is used to compute the state feedback $\mathcal{H}_2$ optimal controller $\ddot{\boldsymbol{d}}_{B,d}^E = -K_p s_p$ for the state cost matrix C_p and input cost matrix D_p. The desired thrust f_Σ and thrust direction $\boldsymbol{z}_{B,d}^E$ are then computed from the desired acceleration.

$$f_\Sigma = m_\Sigma ||\ddot{\boldsymbol{d}}_{B,d}^E - \boldsymbol{g}^E||_2, \; \boldsymbol{z}_{B,d}^E = \frac{\ddot{\boldsymbol{d}}_{B,d}^E - \boldsymbol{g}^E}{||\ddot{\boldsymbol{d}}_{B,d}^E - \boldsymbol{g}^E||_2} \tag{15}$$

4.2 Attitude control

For the inner (attitude) controller, we propose to apply a nonlinear controller based on Mueller (2018). The controller gains are chosen by the desired first-order behavior, described here in terms of the Euler angles that define the rotation from the desired attitude to the current attitude $(\phi_e, \theta_e, \psi_e)$. The desired attitude is defined as that attitude at which the yaw angle of the vehicle matches the desired yaw angle and at which the thrust direction of the vehicle matches the desired thrust direction $\boldsymbol{z}_{B,d}^E$. The angular velocity error $\boldsymbol{\omega}_e^B = (p_e, q_e, r_e)$ is defined as the difference between the desired and true angular velocity of the vehicle. Recall that $\Delta\omega_W = \omega_W - \bar{\omega}_W$ represents the difference between the true and desired angular velocity of the momentum wheel.

As derived in Sect. 2.3, the rotational dynamics decouple into two independent subsystems: one related to the roll and pitch of the vehicle, and another related to the yaw and angular velocity of the momentum wheel. The states relating to the roll and pitch of the vehicle are a subset of the states s_{xy} as given in (4) and (7), and form the rotational subsystem $\dot{s}_{\phi,\theta} = A_{\phi,\theta} s_{\phi,\theta} + B_{\phi,\theta} u_{\phi,\theta}$. The states are $s_{\phi,\theta} = (\phi_e, \theta_e, p_e, q_e)$, inputs $u_{\phi,\theta} = (\tau_x, \tau_y)$, and system matrices defined as follows, where A_2 is given in (10):

$$A_{\phi,\theta} = \begin{bmatrix} 0 & I \\ 0 & A_2 \end{bmatrix}, \qquad B_{\phi,\theta} = \begin{bmatrix} 0 \\ J_{\Sigma,xx}^{-1} I_{2\times 2} \end{bmatrix} \tag{16}$$

Due to vehicle symmetry, the state costs are chosen such that roll and pitch are penalized equally, as are the input torques about $\boldsymbol{x}_B$ and $\boldsymbol{y}_B$. We choose not to explicitly penalize the angular velocity, and thus have the output error $z_{\phi,\theta} = C_{\phi,\theta} s_{\phi,\theta} + D_{\phi,\theta} u_{\phi,\theta}$, where

$$C_{\phi,\theta} = c_{\phi,\theta}\, \mathrm{diag}\,(1, 1, 0, 0) \tag{17}$$

$$D_{\phi,\theta} = d_{\phi,\theta} \mathrm{diag}\,(0, 0, 1, 1) \tag{18}$$

The state feedback $\mathcal{H}_2$ optimal controller $u_{\phi,\theta} = -K_{\phi,\theta} s_{\phi,\theta}$ is defined by $K_{\phi,\theta} = (D_{\phi,\theta}^T D_{\phi,\theta})^{-1} B_{\phi,\theta}^T P$, where P is the solution to the relevant continuous time algebraic Riccati equation (Anderson and Moore, 1989). The solution for $K_{\phi,\theta}$ can be tediously computed by solving the Riccati equation symbolically in terms of the system parameters (e.g. the mass moments of inertia of the system) and the cost weights. Solving for

$K_{\phi,\theta}$ in this way allows for the state feedback $\mathcal{H}_2$ optimal attitude controller to be computed on-the-fly for any given momentum wheel speed, system parameters, and state and input costs. Note that this is applicable only if the wheel speed changes quasi-statically: otherwise, a time-varying controller may be required at the expense of increased computational cost.

$$K_{\phi,\theta} = \begin{bmatrix} \alpha & \beta & \gamma & 0 \\ -\beta & \alpha & 0 & \gamma \end{bmatrix} \tag{19}$$

where

$$L = J_{W,zz}\bar{\omega}_W \ , \quad H = \frac{c_{\phi,\theta}}{d_{\phi,\theta}}\sqrt{16J_{\Sigma,xx}^2 + L^4} - L^2 \tag{20}$$

$$\alpha = \frac{H}{4J_{\Sigma,xx}} \ , \quad \beta = \frac{L\sqrt{2H}}{4J_{\Sigma,xx}} \ , \quad \gamma = \frac{\sqrt{2H}}{2} \tag{21}$$

The controller for the yaw subsystem s_ψ given by (6) and (9) is computed using on the state and input cost matrices C_ψ and D_ψ. As this subsystem is not affected by the wheel speed $\bar{\omega}_W$, the gain matrix K_ψ may be computed offline.

After the desired total thrust f_Σ and input torques $\boldsymbol{\tau}_u^B = (\tau_x, \tau_y, \tau_z)$ have been computed, the propeller thrusts (and thus speeds) required to achieve these forces and torques are computed. This mapping is dependent on the structure of the multicopter and will change depending on the number and position of propellers. For example, the desired individual propeller thrusts for a quadcopter are computed by inverting (3).

4.3 Sensitivity to estimated wheel speed error

Errors between the estimated wheel speed and true wheel speed can result in a greater sensitivity of the system to disturbances or even outright instability. Figure 5 shows how the torque disturbance sensitivity of the system defined by (4) and (7) changes as a function of the difference between the estimated wheel speed and a true wheel speed of $\omega_W = 468\,\mathrm{rad\,s^{-1}}$ using the parameters of the larger vehicle shown in Fig. 1. The $\mathcal{H}_2$ cost is normalized by the sensitivity of the system with $\omega_W = 0$, and is evaluated for both the $\mathcal{H}_2$ optimal state feedback controller considered in Sect. 3.1 and the cascaded controller presented in this section.

The naïve full-state $\mathcal{H}_2$ optimal controller results, of course, in the lowest system sensitivity to torque disturbances. However, this controller shows extreme sensitivity to errors in the belief of the estimated wheel speed, and the closed-loop system becomes unstable even for a very small over-estimation of the wheel speed. The cascaded controller, on the other hand, does not show this sensitivity to estimation errors, but has a greater

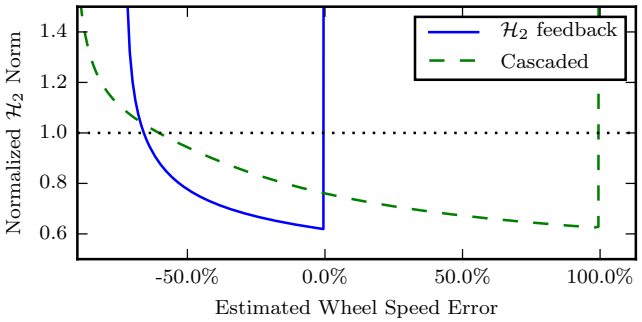

Fig. 5 Sensitivity of the vehicle to roll/pitch torques as a function of the error of the estimated wheel speed for the large quadcopter with a true wheel speed of $\omega_W = 468\,\mathrm{rad\,s^{-1}}$. The $\mathcal{H}_2$ cost is normalized such that any value less than 1 indicates the vehicle is less sensitive to roll/pitch torque disturbances than a vehicle with $\omega_W = 0$.

closed-loop sensitivity to the disturbances, although it should be noted that this is not necessarily due to the cascaded nature of the controller. In fact, the sensitivity of the naïve full-state controller to estimation errors can be changed by modifying the costs associated with each state (including adding cost to the angular velocity states), but it is unclear how these costs would be chosen such that acceptable sensitivities to both estimation errors and disturbances are simultaneously achieved. Furthermore, although the cascaded controller presented in this section is not the optimal controller in terms of improving the disturbance sensitivity of the system, it is still useful due to relative insensitivity to errors in the estimated wheel speed, ease of implementation, and its ability to straight-forwardly cope with large attitude errors.

5 Experimental Validation

In this section we present experimental results to validate the models using two vehicles of different scales subjected to torque impulse disturbances. An additional test case is presented where the torque impulse disturbance is large enough to cause saturation of the motor forces. The improvement of the yaw control authority of the vehicle is verified by commanding a step change in yaw.

5.1 Platform

Two custom quadcopters of different sizes were constructed for testing as shown in Fig. 1, with masses differing by a factor of 18. The smaller vehicle uses CL-0720-14 brushed motors while the larger vehicle uses EMAX MT2208 brushless motors with DYS SN30A electronic speed controllers that control the rotational

Table 1 Physical parameters of experimental vehicles

Parameter	Large Vehicle	Small Vehicle
m_Σ	922 g	50 g
$J_{\Sigma,xx}$	5.8×10^{-3} kg m^2	3.5×10^{-5} kg m^2
$J_{\Sigma,zz}$	10.7×10^{-3} kg m^2	6.0×10^{-5} kg m^2
$J_{W,zz}$	6.4×10^{-4} kg m^2	1.7×10^{-6} kg m^2
$f_{P_i,max}$	6.86 N	0.24 N
$\|\|\boldsymbol{r}_i\|\|_2$	0.166 m	0.048 m
$\|\kappa_i\|$	0.014 m	0.001 m

Table 2 Parameters used to compute control cost matrices

Parameter	Value
$\|l_{max}\|$	2.5 m
$\|a_{max}\|$	10 m s^{-2}
$\|\phi_{e,max}\|, \|\theta_{e,max}\|, \|\psi_{e,max}\|$	30°
$\|\Delta\omega_{W,max}\|$	50 rad s^{-1}
$\|\tau_{x,max}\|, \|\tau_{y,max}\|$	$\|r_{i,x}\|f_{P_i,max}$
$\|\tau_{z,max}\|$	$\|\kappa_i\|f_{P_i,max}$
$\|\tau_{W,max}\|$	$5\|\tau_{z,max}\|$

velocity of the motors in closed-loop. The same motors and speed controllers are used to spin the momentum wheel on each vehicle. The physical parameters of each vehicle are listed in Table 1.

We compare the responses of each vehicle both with and without their momentum wheels spinning. For the large vehicle, the nominal wheel speed is set to $\bar{\omega}_W = 468\,\text{rad}\,\text{s}^{-1}$, determined based upon an energy argument: At this speed, the rotational energy stored in the momentum wheel is twice the maximum rotational energy stored in the propellers of the vehicle, meaning that the addition of the momentum wheel does not radically change the danger posed by the vehicle's rotating parts. For the smaller vehicle, the nominal wheel speed is set to $\bar{\omega}_W = 1000\,\text{rad}\,\text{s}^{-1}$. At this scale, the rotational energy is not a concern, and this speed was chosen to be slightly below the maximum that can be achieved by the driving motor.

For the shown experiments, the position and attitude of the quadcopter are measured directly by an external motion capture system, and the angular velocity of the quadcopter is measured using an onboard rate gyroscope. The position controller runs on an offboard computer and sends commands and attitude measurements to the quadcopter via radio at 50Hz. The attitude controller is ran onboard the quadcopter at 500Hz. The use of other sensing technologies (e.g. GPS) are expected to yield similar results, while even more pronounced improvements may result if onboard vision is used, where estimation performance is degraded through motion blur.

5.1.1 Control

The $\mathcal{H}_2$ error weights for the cascaded controller of Sect. 4 were chosen using Bryson's rule (Bryson and Ho, 1975), which is a heuristic based on the maximum acceptable values of the states and inputs, so that the output errors are normalized to their maximum acceptable values. For example, for a maximum roll error $\phi_{e,max}$, a cost weighting $c_{\phi,\theta} = \phi_{e,max}^{-1}$ is used. The cost weighting are then used to compose state the cost matrices C_p, $C_{\phi,\theta}$, C_ψ and input cost matrices D_p, $D_{\phi,\theta}$, D_ψ, which are used to compute corresponding the state feedback $\mathcal{H}_2$ optimal controllers as described in Sect. 4. We use l_{max} as the maximum acceptable position error, a_{max} is the maximum acceptable acceleration, and again weight the two horizontal axes similarly due to the symmetry of the vehicle. The maximum acceptable values used to compute each cost matrix are given in Table 2.

In addition to the cascaded feedback controller, a small feedforward term is added to τ_z to compensate for the drag torque exerted by the momentum wheel about its axis of rotation $\boldsymbol{z}_B$ as it spins. This drag torque is not included in the system model (9), and thus must be determined experimentally.

5.1.2 Power Consumption

Using the relationship described in Sect. 3.2 to calculate the mechanical power required to lift a given mass, the larger vehicle requires 58 W of mechanical power to hover when the momentum wheel is not attached. However, when the momentum wheel is attached, an additional 100 g is added to the mass of the vehicle, requiring an additional 11 W of mechanical power to hover. Furthermore, 4.8 W of mechanical power is required to spin the wheel at the desired speed of 468 rad s^{-1}, resulting in a 27% increase in power consumption when the wheel is attached and spinning compared to a vehicle without the wheel attached. The mechanical power required to spin the wheel is composed of the power consumed by the motor spinning the wheel (used to overcome aerodynamic drag acting on the spinning wheel), and the additional power consumed by the propellers (used to compensating for the torque produced by the wheel motor). The electrical power consumed will of course be larger, due to losses in the power train, but the relative increase should be approximately the same.

The increase in power consumption due to the momentum wheel is similar for the smaller vehicle. Without the wheel the vehicle produces 0.54 W of mechanical power during hover, and the attached 3.9 g momentum wheel requires and additional 0.07 W to lift and 0.05 W to spin at 1000 rad s^{-1}, corresponding to an increase in power consumption of 23%. Optimized designs may be expected to perform substantially better than this.

Fig. 6 Test vehicles with attached arm extensions. A falling mass collides with the arm extension in order to provide an torque impulse disturbance to the vehicle.

5.2 Impulse torque disturbance rejection

The torque disturbance rejection capabilities of each vehicle are tested by applying a repeatable torque impulse to the vehicle by dropping a mass on the vehicle from above. Arm extensions are added to each vehicle as shown in Fig. 6 so that the falling mass does not collide with the propellers of the vehicle. For the larger vehicle, masses of 67 g and 135 g were dropped from a height of 1 m to apply torque impulses of 0.092 N m s and 0.186 N m s to the vehicle respectively. For the smaller vehicle, a mass of 5 g was dropped from a height of 5 cm to apply an estimated torque impulse of 4.7×10^{-4} N m s to the vehicle. Figure 7 shows the responses of each vehicle to these torque impulse disturbances, and Fig. 8 shows a sequence of images corresponding to the response of the larger vehicle to the 0.186 N m s torque impulse disturbance. The attached video shows how the experiments are performed.

In each of the experiments, the improvement due to the momentum wheel is clear: A lower peak tilt error is recorded, smaller horizontal and vertical errors occur, and the required thrust forces are lower. The improvement of the response of the vehicle with the wheel spinning over the vehicle without the wheel spinning is particularly clear for the large impulse on the larger vehicle, shown in Fig. 7b, being large enough to cause the thrust forces to saturate only when the wheel is not spinning.

We compare the responses of the vehicles by computing the experimental state feedback $\mathcal{H}_2$ cost of the system trajectory for each test; that is we integrate (11) over $t \in [0, 2.5]$ using a position cost of $1\,\mathrm{m}^{-1}$ and roll/pitch torque cost of $1\,\mathrm{N}^{-1}\,\mathrm{m}^{-1}$. For the large vehicle's test cases shown in Figs. 7a and 7b, the experimental cost when using the wheel is 0.54 and 0.32 respectively when normalized to the cost when the wheel is not used. This experimentally observed normalized cost is comparable to that predicted by the analytic model of 0.62, with the discrepancy likely due to modeling errors and actuator saturation in the case of Fig. 7b. The smaller vehicle's experimentally observed performance exceeds that predicted, most likely due to (comparatively) poor position tracking for the smaller vehicle. Moreover, the presence of sensor/environmental noise in the system (in addition to the initial impulse), means that the experimental cost is affected by the choice of integration length (with the theoretical result corresponding to a noise-free impulse response integrated over an infinite horizon). The analytic model also does not account for any aerodynamic effects that may be introduced by the spinning of the momentum wheel, and in general it is difficult to predict such effects.

5.3 Improved yaw authority

Although the magnitude of the angular momentum stored in the momentum wheel does not affect the sensitivity of the vehicle to torque disturbances about the yaw axis, the wheel can be used to improve the yaw authority of the vehicle as discussed in Sect. 4.2. Specifically, the motor driving the wheel provides an additional yaw torque that results in the wheel either accelerating or decelerating relative to the vehicle body. The improvement in yaw authority is experimentally validated by commanding 45° step changes in desired yaw in both the positive and negative directions while the vehicle is hovering. Results are compared to the response of the vehicle performing the same maneuver without allowing the momentum wheel to accelerate or decelerate, which is accomplished by setting $\Delta\omega_{W,max} = 0$ instead of $\Delta\omega_{W,max} = 50\,\mathrm{rad\,s}^{-1}$ as given in Table 2 and recomputing the associated cost matrices C_ψ and D_ψ used to compute the gain matrix K_ψ as described in Sect. 5.1.1. A response to a single trial for the large vehicle is shown in Fig. 9, as well as in the video attachment.

The magnitude of the improvement of the yaw authority is dependent on both the limits on the torque of the motor driving the momentum wheel, and on the tolerable change in the speed of the wheel. Note, however, that the range of τ_W can be asymmetric due to the actuators used to drive the wheel. For example, on the smaller vehicle the wheel is driven by a unidirectional brushed motor, meaning that the wheel can be accelerated by the motor, but must rely on friction and drag torque to decelerate the wheel.

Although the controller described in Sect. 4.2 uses the torque produced by the motor driving the wheel as a control input, electronic speed controllers (including those used in these experiments) commonly required speed commands. In order to compute the desired speed command $\bar{\omega}_W$ for the momentum wheel motor such that

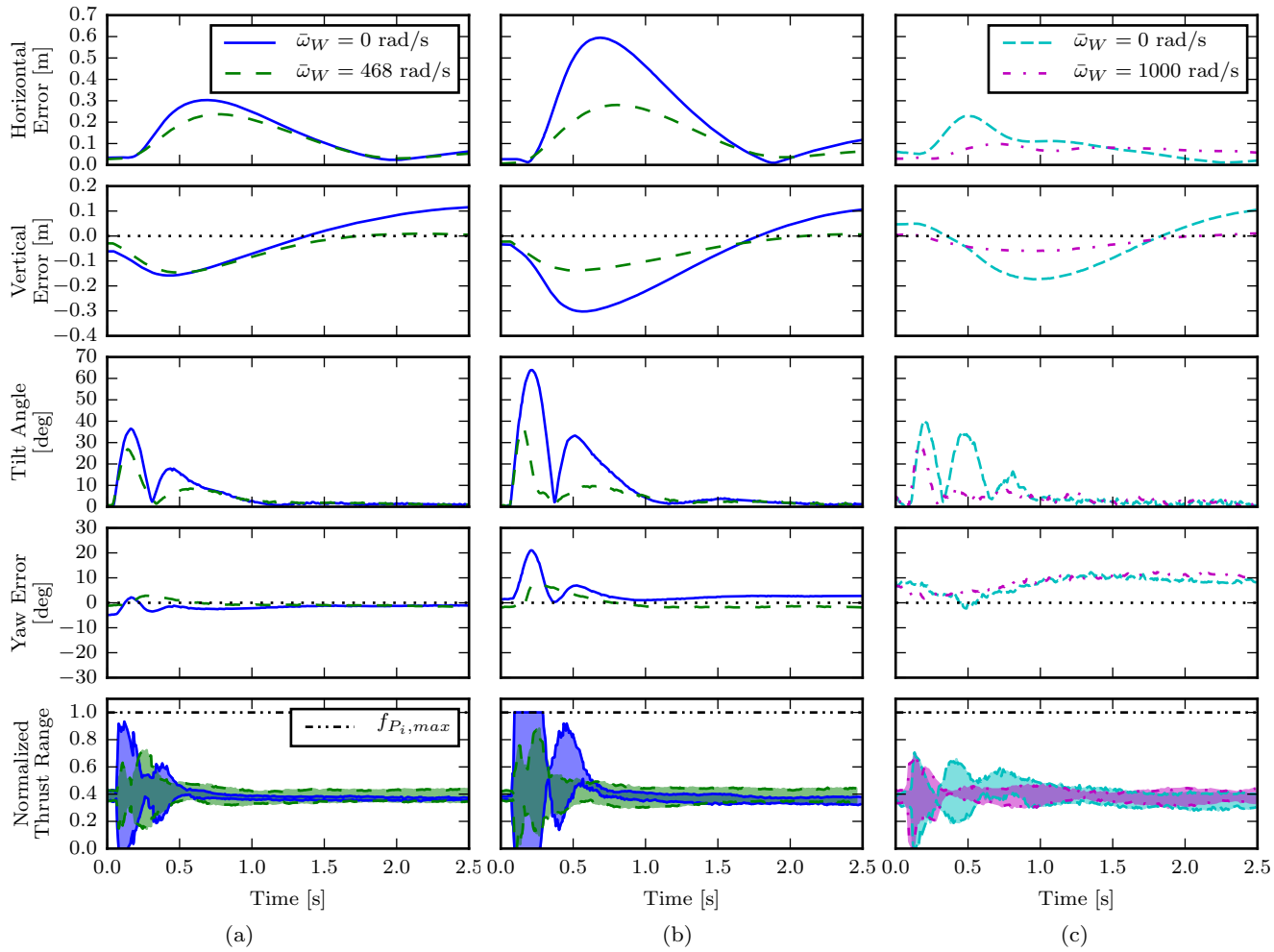

Fig. 7 Responses to a torque impulse caused by a collision with a mass dropped from above. The tilt angle is defined as the angle between $\boldsymbol{z}_B^E$ and the vertical, and the normalized thrust range is defined as the minimum range that contains all four thrust forces, which are normalized to the maximum thrust $f_{P_i,max}$. The response of the larger vehicle to a 0.092 N m s torque impulse is shown in (a), the response of the larger vehicle to a 0.186 N m s torque impulse is shown in (b), and the response of the smaller vehicle to a 4.7×10^{-4} N m s torque impulse is shown in (c). The performance of the vehicle is improved in all three cases when the wheel is spinning, and an even more significant improvement is observed when the motor forces saturate, as shown in (b). A video of the experiments is attached to the paper.

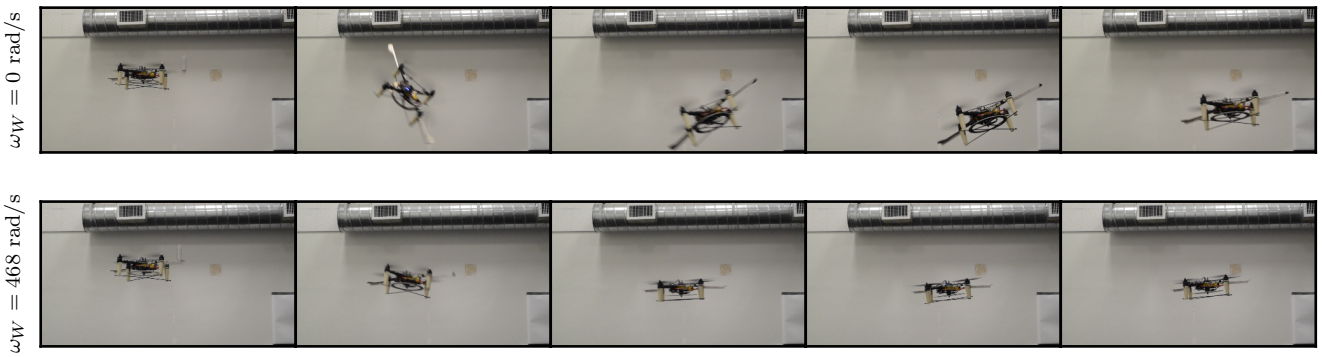

Fig. 8 Response of the larger vehicle to a 0.186 N m s torque impulse as shown in Figure 7b. The top series of images shows the response without the momentum wheel spinning, and the bottom series of images shows the response when the momentum wheel is spinning at 468 rad s^{-1}. Images are spaced 0.2 seconds apart, and are taken from the video attachment to this paper.

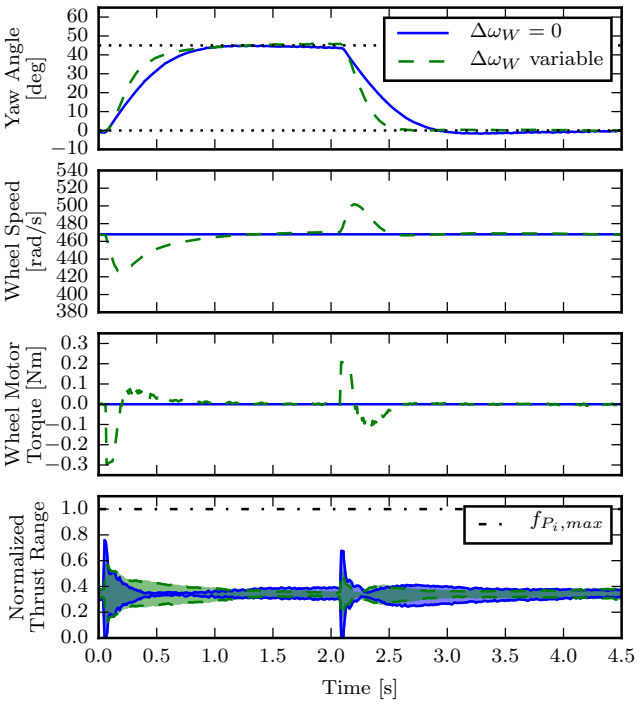

Fig. 9 Response of the large vehicle to a step change in desired yaw of 45° followed by a second step change in desired yaw back to 0°. A controller that allows for some error in the desired momentum wheel speed outperforms a controller that does not allow the wheel to accelerate or decelerate.

the desired torque τ_W is applied, we model the speed of the wheel ω_W as a first order system as follows, where c is the time constant of the wheel (we estimated $c \approx 1\,\text{s}$ for the large vehicle).

$$\dot{\omega}_W = \frac{1}{c}(\bar{\omega}_W - \omega_W) \tag{22}$$

Given a desired torque, the desired speed command for the momentum wheel motor is then computed as

$$\bar{\omega}_W = \omega_W + \frac{c}{J_{W,zz}}\tau_W \tag{23}$$

5.4 Step change in position

In order to compare how additional angular momentum affects the maneuverability of the vehicle, the responses of the larger vehicle to a 1.5 m horizontal step change in desired position both with and without the momentum wheel spinning are compared in Fig. 10. The sudden change in desired thrust direction also results in a sudden change in desired attitude of the vehicle.

Due to the angular momentum of the wheel, more time is required to change the attitude of the vehicle when the wheel is spinning. However, because the majority of the maneuver consists of translating rather than rotating, the responses of the vehicles with and without the wheel spinning are similar, where the vehicle with the wheel spinning requires slightly more time to reach the desired position.

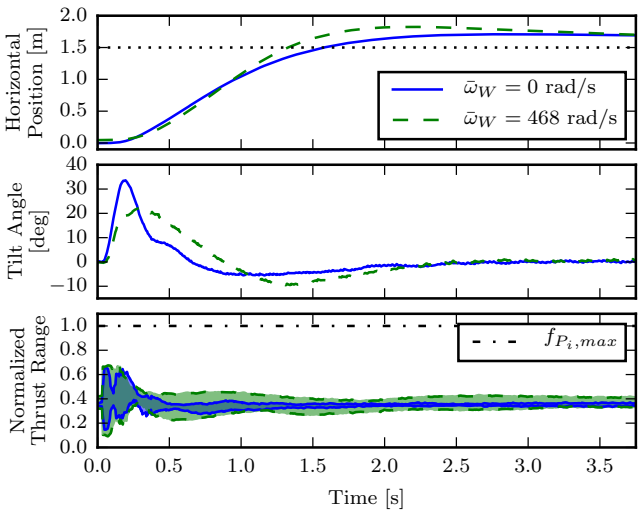

Fig. 10 Responses of the large vehicle to a 1.5 m horizontal step change in desired position both with and without the momentum wheel spinning. The vehicle with the wheel spinning requires slightly more time to reach the desired position.

6 Conclusion

In this paper we have presented a novel design for a multicopter for use in challenging environments, exploiting the addition of a momentum wheel for increased robustness to disturbances. The vehicle dynamics were derived, of which the additional coupling between the vehicle's roll and pitch dynamics is key to the added robustness. A scaling analysis shows that greater benefit is expected for smaller vehicles. A simple cascaded control structure is proposed and implemented in experiment; the experimental results are shown to correspond closely to that predicted by the analysis of the system.

Specifically, it is shown that as the angular momentum of the wheel is increased, the vehicle's position tracking $\mathcal{H}_2$ cost monotonically decreases for torque disturbances. For force disturbances, the cost initially also decreases, but is shown to increase when the wheel has large angular momentum. As the momentum wheel speed can be varied dynamically in flight, the vehicle's flight characteristics can be adapted mid-mission, allowing e.g. for agile motion followed by steady station keeping.

This increase in robustness comes at additional energetic cost associated with increasing the vehicle mass, though the amount of added mass can be reduced at the

cost of increasing the kinetic energy stored in the wheel. Furthermore, we show that the closed-loop system may be extremely sensitive to errors in belief of the wheel speed, but the proposed cascaded controller is shown to be less sensitive than a naïve full state linearized feedback controller.

Vehicles of the proposed design may be expected to be especially valuable when conducting missions in very sensitive or unpredictable environments, such as when operating over crowds of people, or near critical infrastructure. Future implementations may consider replacing the momentum wheel with a large propeller, allowing the vehicle to increase the propellers' surface area and potentially increasing overall system efficiency; other designs may enclose the momentum wheel in a very robust cage, allowing the wheel to operate at very high velocities with low mass.

Acknowledgements This material is based upon work supported by the National Science Foundation Graduate Research Fellowship under Grant No. DGE 1752814 and the Powley Fund.

References

Anderson B, Moore J (1989) Optimal Control: Linear Quadratic Methods. Prentice-Hall International

Besnard L, Shtessel YB, Landrum B (2012) Quadrotor vehicle control via sliding mode controller driven by sliding mode disturbance observer. Journal of the Franklin Institute 349(2):658–684

Bryson A, Ho YC (1975) Applied Optimal Control: Optimization, Estimation and Control. CRC Press

Bucki N, Mueller MW (2018) Improved quadcopter disturbance rejection using added angular momentum. In: Intelligent Robots and Systems (IROS), 2018 IEEE/RSJ International Conference on, IEEE

Cabecinhas D, Cunha R, Silvestre C (2014) A nonlinear quadrotor trajectory tracking controller with disturbance rejection. Control Engineering Practice 26:1–10

Driessens S, Pounds P (2015) The triangular quadrotor: a more efficient quadrotor configuration. IEEE Transactions on Robotics 31(6):1517–1526

Green M, Limebeer D (1995) Linear Robust Control. Dover Publications

Kushleyev A, Mellinger D, Powers C, Kumar V (2013) Towards a swarm of agile micro quadrotors. Autonomous Robots 35(4):287–300

Likins PW (1967) Attitude stability criteria for dual spin spacecraft. Journal of Spacecraft and Rockets 4(12):1638–1643

McCormick BW (1995) Aerodynamics Aeronautics and Flight Mechanics. John Wiley & Sons, Inc

Mingori D (1969) Effects of energy dissipation on the attitude stability of dual-spinsatellites. AIAA Journal 7(1):20–27

Mueller MW (2018) Multicopter attitude control for recovery from large disturbances. CoRR abs/1802.09143, URL `http://arxiv.org/abs/1802.09143`, `1802.09143`

Mueller MW, D'Andrea R (2014) Stability and control of a quadrocopter despite the complete loss of one, two, or three propellers. In: IEEE International Conference on Robotics and Automation (ICRA)

Mueller MW, D'Andrea R (2016) Relaxed hover solutions for multicopters: Application to algorithmic redundancy and novel vehicles. The International Journal of Robotics Research 35(8):873–889

Piccoli M, Yim M (2014) Passive stability of a single actuator micro aerial vehicle. In: Robotics and Automation (ICRA), 2014 IEEE International Conference on, IEEE, pp 5510–5515

Piccoli M, Yim M (2015) Passive stability of vehicles without angular momentum including quadrotors and ornithopters. In: 2015 IEEE International Conference on Robotics and Automation (ICRA), IEEE, pp 1716–1721

Pounds P, Mahony R, Hynes P, Roberts JM (2002) Design of a four-rotor aerial robot. In: Proceedings of the 2002 Australasian Conference on Robotics and Automation (ACRA 2002), Australian Robotics & Automation Association, pp 145–150

Ryll M, Bülthoff HH, Giordano PR (2013) First flight tests for a quadrotor UAV with tilting propellers. In: 2013 IEEE International Conference on Robotics and Automation (ICRA), IEEE, pp 295–302

Wallace DA (2016) Dynamics and control of a quadrotor with active geometric morphing. Master's thesis

Waslander S, Wang C (2009) Wind disturbance estimation and rejection for quadrotor position control. In: AIAA Infotech@ Aerospace Conference and AIAA Unmanned... Unlimited Conference, p 1983

Zhang R, Quan Q, Cai KY (2011) Attitude control of a quadrotor aircraft subject to a class of time-varying disturbances. IET control theory & applications 5(9):1140–1146

Zhang W, Mueller MW, D'Andrea R (2016) A controllable flying vehicle with a single moving part. In: 2016 IEEE International Conference on Robotics and Automation (ICRA), IEEE, pp 3275–3281

Zipfel PH (2007) Modeling and Simulation of Aerospace Vehicle Dynamics, 2nd edn. American Institute of Aeronautics and Astronautics